



## REVIEW ARTICLE

# Interferometric Synthetic Aperture Radar

Christopher T. Allen

Department of Electrical Engineering and Computer Science and  
Radar Systems and Remote Sensing Laboratory  
University of Kansas

**Abstract.** This paper provides a brief review of interferometric synthetic aperture radar (InSAR), its history, the theory, and design / implementation / processing issues. Along-track, single-pass and repeat-pass cross-track interferometry are reviewed. Specific topics addressed include error sources and phase-unwrapping techniques. Several examples of InSAR applications are presented.

## Introduction

For years synthetic aperture radar (SAR) has been used to produce photograph-like images of terrain features. Conventional SAR systems provide a two-dimensional map of the radar reflectivity of the illuminated scene. While complex data are collected and processed to produce the SAR image, one of the final steps in its production is to reduce a complex image (containing both magnitude and phase information) to a purely magnitude image, with the phase information being discarded.

Radar interferometry, on the other hand, depends on phase information. Through interferometry, range information can be resolved to less than a wavelength. However, interferometry brings with it range ambiguities that limit its usefulness.

Together, SAR and interferometry provide additional information to that of a conventional SAR. Depending on the implementation, interferometric SAR, or InSAR, can survey height information of the illuminated scene, measure the radial velocity of moving scatterers, track subtle terrain motions, or detect slight changes in scene content.

## History

*Graham* [1974] first demonstrated interferometric SAR by using an airborne SAR system configured as a cross-track or vertical interferometer. He used two vertically separated antennas to receive simultaneously backscattered signals from the terrain. Vectorial addition of these signals produced a pattern of nulls corresponding to predetermined depression angles, which, when used in conjunction with range information, yielded elevation information. He recorded data optically from two channels: one was the normal SAR data; the other, the interferometer output containing the null patterns. He showed that since the multiple nulls were ambiguous, the elevation of at least one point within the scene must be determined by an alternate means to resolve the absolute elevation.

*Goldstein and Zebker* [1987] first employed an along-track

interferometric SAR configured to measure radial velocity. They used two horizontally separated antennas to receive backscattered signals from the moving sea surface. They processed the signals separately to form two complex images, which they then combined interferometrically; i.e., the phases were differenced pixel by pixel. They showed that since radial motion of a surface scatterer causes a phase difference between the two images that is proportional to the distance moved, scatterer motion can be measured.

*Gabriel and Goldstein* [1988] first demonstrated single-antenna, repeat-pass interferometry by using data collected on two separate passes of the Shuttle Imaging Radar (SIR-B). Despite the fact that the orbits were skewed, through refocussing and careful image registration, they obtained an altitude map of the imaged region.

## Theory

Whereas conventional SAR uses a single antenna, InSAR requires two antennas separated by a baseline ( $B$ ). Signals from both antennas are recorded and processed to yield two complex SAR images of the same scene. Phases measured in each of the scenes are differenced on a pixel-by-pixel basis to obtain additional geometrical information about the scene.

When the receive antennas are vertically separated, this phase difference can be interpreted as pixel height as illustrated in Figure 1. Pixel height,  $h$ , and phase difference,  $\phi$  are related by [*Li and Goldstein*, 1990]:

$$\phi = \frac{2\pi}{\lambda} [B_x \sin \theta - B_y \cos \theta] \quad (1)$$

$$h = H - \rho(\cos \theta) \quad (2)$$

where the parameters are those shown in Fig. 1 and  $\lambda$  is the radar wavelength.

Equations (1) and (2) assume a single-pass system; i.e., a single transmit antenna and dual receive antennas. When repeat-pass interferometry is used, the  $2\pi$  term in (1) should be replaced by  $4\pi$

When the receive antennas are separated horizontally along the radar velocity vector (along-track InSAR), phase differences can be interpreted as scatterer motion proportional to the radial distance moved in the time required for the rear antenna to move to the position previously occupied by the forward antenna [*Goldstein and Zebker* 1987]. The phase difference and the radial velocity of the scatterer are related by

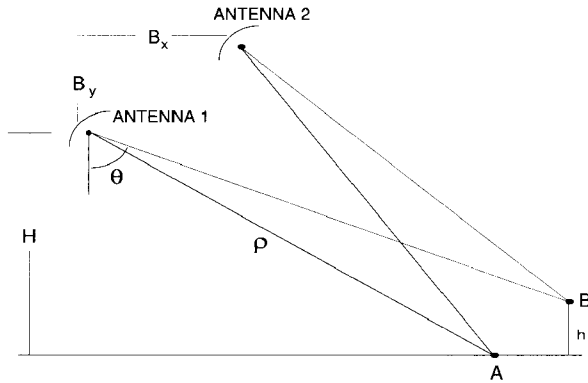


Figure 1. Typical geometry of a cross-track interferometric SAR. Targets A and B are at the same azimuth and slant range to antenna 1. In conventional SAR, where only one antenna is used, the returns from A and B are projected into the same pixel. In the InSAR configuration both antennas are used and a phase difference between antennas 1 and 2 can be used to derive the height for each pixel. (after Li and Goldstein [1990])

$$\phi = \frac{4\pi u B}{\lambda v} \quad (3)$$

where lambda is the radar wavelength, B is the baseline distance between antennas, v is the radar velocity and u is the radial velocity of the scatterer.

Regardless of antenna configuration, the processing begins with a pair of complex pixel values,  $v_1$  and  $v_2$ , that contain the interferometric data. Working prior to the availability of digital processing techniques, Graham [1974] used an analog vector addition process (described by Ulaby, Moore, and Fung [1982]) to produce null patterns that revealed the pixel elevation information. Another approach is to measure the phase difference of the signal between each complex pixel pair. The maximum-likelihood estimator (MLE) that provides this phase difference for distributed, homogeneous targets is

$$\hat{\phi} = \arctan \left[ \frac{\text{Im} \left\{ \sum_{n=1}^{N_L} v_1^{(n)} v_2^{*(n)} \right\}}{\text{Re} \left\{ \sum_{n=1}^{N_L} v_1^{(n)} v_2^{*(n)} \right\}} \right] \quad (4)$$

where  $N_L$  is the number of looks to be averaged [Rodriguez and Martin, 1992] and \* denotes the complex conjugate. This technique is widely used today.

### Error Sources

The relationships presented above assume ideal conditions. For example, in developing (3), it is assumed that the antennas

are collinear. Should this not be the case, an additional phase difference unrelated to scatterer motion will arise.

Similarly, a variety of error sources will corrupt the pixel height estimate [Li and Goldstein, 1990]. Differentiating (1) and (2) with respect to each parameter, height uncertainties due to each parameter are obtained. The pixel height uncertainty due to uncertainties in range,  $\rho$ , due to system clock timing, data-sampling clock jitter, atmospheric propagation delay, etc., is

$$\sigma_h^1 = \sigma_\rho \cos \theta. \quad (5)$$

Height uncertainty due to uncertainties in system attitude and baseline separation are

$$\sigma_h^2 = \frac{\rho (\sin \theta)^2}{(B_x \cos \theta + B_y \sin \theta)} \sigma_{B_x} \quad (6)$$

$$\sigma_h^3 = \frac{\rho \sin \theta \cos \theta}{(B_x \cos \theta + B_y \sin \theta)} \sigma_{B_y}. \quad (7)$$

Uncertainties in system altitude contribute to pixel height uncertainty as

$$\sigma_h^4 = \sigma_H. \quad (8)$$

Finally, phase measurement uncertainty contributes to pixel height uncertainty as

$$\sigma_h^5 = \frac{\lambda \rho \sin \theta}{2\pi (B_x \cos \theta + B_y \sin \theta)} \sigma_\phi. \quad (9)$$

The major contributors to phase measurement uncertainty are signal-to-noise ratio, speckle, pixel misregistration, and decorrelation. Noise will corrupt the phase measurement and, hence, the signal-to-noise ratio will determine the measurement uncertainty. When a resolution cell contains multiple scatterers, the random coherent interference that gives rise to the fading phenomenon will also result in speckle. Like noise, this also will degrade the phase measurement. Similarly, pixel misregistration between the two complex SAR images to be differenced will result in a lack of coherency at the pixel level resulting in degraded phase measurement.

Decorrelation refers to three additional sources of phase measurement uncertainty: baseline decorrelation, decorrelation due to target rotation, and decorrelation from surface motion of individual scattering centers within a resolution cell [Zebker and Vollasenor, 1992]. The same effect that gives rise to the fading phenomenon will also result in differing phase measurements when a distributed scatterer is viewed from antennas separated by the baseline. This is referred to as



baseline decorrelation. Likewise, when a complex collection of scatterers is viewed from two different aspect angles, a decorrelation of the phase measurement will result, attributed to target rotation. Finally, should the arrangement of scatterers physically change between observations, this will result in temporal decorrelation. Temporal decorrelation may be significant in repeat-pass InSAR.

The degree of decorrelation (due to the causes listed above) between two complex SAR images can be measured and is called the coherence. Given a pair of complex pixel values,  $v_1$  and  $v_2$ , coherence is defined as [Askne and Hagberg 1993]

$$\gamma = \frac{E[v_1 v_2^*]}{\sqrt{E[v_1 v_1^*]E[v_2 v_2^*]}} \quad (10)$$

where  $E[\dots]$  represents ensemble averaging. An estimate of coherence,  $\gamma$ , can be obtained through spatial averaging.

Phase aberrations may arise during data acquisition or during data processing. Stevens et al. [1993] and Stevens, Cumming, and Gray [1994] examine the unique motion compensation requirements of an airborne InSAR. Atmospheric refraction can also introduce phase aberrations for both single-pass and repeat-pass spaceborne InSAR. Tarayre and Massonnet [1994] examined the effect of spatial and temporal fluctuations of both the troposphere and the ionosphere and simulated the effects on an interferogram, finding that for microwave frequencies both misregistration and phase artifacts can result. To compensate for these effects, they developed a concept of fictive satellite positions and reduced the worst-case misregistration from about 15 m to less than 3 cm and reduced the effects of phase artifacts from a worst case of about 6 m to less than 2 cm.

### Double Difference

Gabriel, Goldstein, and Zebker [1989] introduced the concept of differential interferometric SAR, a technique capable of detecting very small elevation changes over large areas. Two interferograms made from three (or more) complex SAR images collected at different times are differenced producing a third interferogram, termed a "double-difference interferogram." Phase changes due to static topography are removed, leaving a new phase image with nonzero phases in areas where the surface has been disturbed between observation times. This technique used SEASAT SAR imagery collected over agricultural fields during a 12-day period to reveal elevation changes greater than 3 cm. These elevation changes were attributed to the swelling of water-absorbing clays.

### Phase Characteristics

Phase statistics have been examined and characterized for SAR interferograms. The effect of thermal noise, phase aberrations, and spectral envelope misalignment upon the phase

uncertainty is treated by Just and Balmer [1994]. Multilook processing, frequently used for speckle reduction and data compression, changes the phase characteristics of InSAR data. Lee et al. [1994] derived the probability density functions of magnitude and phase for multilook InSAR measurements. When adjacent pixels are not completely independent, an effective number of looks must replace the nominal number. Examples are provided by Joughin and Winebrenner [1994].

Maximum likelihood estimates for InSAR phase, coherence magnitude, and image sample variance were derived by Seymour and Cumming [1994].

An additional source of phase measurement uncertainty in repeat-pass InSAR occurs when the physical surface characteristics change between observations, known as temporal decorrelation. Zebker and Vollasenor [1992] demonstrated the feasibility of applying repeat-pass InSAR mapping of vegetated and forested areas.

## Processing Issues

### Image Registration

Both single-pass and repeat-pass interferometry require that the two complex SAR images be registered prior to determining the phase difference, and for the repeat-pass mode this step is nontrivial. Skewed radar trajectories and differing look angles complicate the image registration process. Gabriel and Goldstein [1988] addressed the image registration issue when processing data collected from SIR-B on crossing-orbital paths. Proper registration of the two complex SAR images required a resampling of one of the images in both the alongtrack and cross-track directions. Resampling parameters were determined iteratively based on the quality of the interference fringes. Lin, Vesecky, and Zebker [1992] describes a similar image registration process using a second image resampled on a 0.1 x 0.1 pixel grid to determine the optimum registration. The average fluctuation in the phase difference image was the criterion used to measure registration quality in this technique. Kwoh et al. [1994] compared the effectiveness of complex correlation, phase fluctuation, and amplitude correlation techniques and found that for ERS-1 data collected 35 days apart, the latter technique proved to be superior.

### Calibration

InSAR requires relative phase calibration. Freeman [1992] examined the calibration requirements of both single-pass and repeat-pass InSAR. Bickel and Hensley [1994] examined the accuracy of four different techniques for InSAR phase calibration including imaging flat surfaces of known height (such as lake surfaces), laboratory measurements, and in-flight, closedloop calibration. They found the use of a delay line and imaging a lake surface to provide phase inaccuracies of less than 1°.

### Phase Unwrapping

Phase information is measured in modulo 2pi yet height information requires the *whole phase*. A variety of methods



have been reported to *unwrap* the measured phase and remove any ambiguities. Except for problem areas, the two-dimensional phase map from a properly designed InSAR system will be phase continuous; i.e., the true phase changes by less than one-half cycle pixel to pixel. Problem areas include regions where the signal-to-noise ratio is too small due to low reflectivity or shadowing and regions where significant terrain relief results in layover. In addition, speckle will cause local discontinuities. *Goldstein, Zebker, and Werner* [1988] developed a technique for two-dimensional phase-unwrapping that identifies these regions, termed residues. Branch cuts are then defined in conjunction with the identified residues and serve to interdict integration paths, the final step in the phase-unwrapping process. *Prati, Giani, and Leuratti* [1990(a)] examined the phase-unwrapping process and introduced the concept of *ghost lines* that delineate a border between regions across which a phase discontinuity occurs, principally due to steep ascending slopes. *Lin, Vesecky, and Zebker* [1992] approach the problem through a method involving fringe-line detection. This approach requires performing an edge detection and again identifies residue regions. *Guarino* [1994] presented a technique, the instantaneous frequency algorithm, that is reported to be less sensitive to misregistration and to weak signal-to-noise ratios than conventional unwrapping algorithms. This technique involves estimating the phase derivative in two orthogonal directions and then performing a two-dimensional integration. *Lo-eld and Kramer* [1994] developed a technique that simultaneously filters and unwraps the phase with an extended linearized Kalman filter that performs well on simulated InSAR data. A technique for lengthening the phase ambiguity interval has been reported by *Xu et al.* [1994] through the use of multiple InSAR images. Three methods of combining multiple InSAR images were examined and the results compared.

Once the phase is unwrapped, to obtain the absolute pixel height, an absolute phase is required. A point of known elevation within the scene can be used to provide an absolute elevation reference. *Madsen and Zebker* [1992] developed a technique for obtaining the absolute phase of the scene strictly from the radar signal. This method involves splitting the range bandwidth into sub-bands and processing each separately. The result is two SAR images obtained from systems with slight differences in radar frequencies. This frequency difference coupled with the InSAR phase-measurement capability enable the absolute phase to be determined

#### *Processing effects*

While SAR processing can contribute to phase decorrelation, *Cattabeni, Monti-Guarnieri, and Rocca* [1994] showed that through a *tuning* process decorrelation due to misregistration and defocusing can be minimized and phase accuracy can be improved. The approach also addresses a means to reduce volume scattering decorrelation.

#### *Slant-Range Resolution Improvement*

Using the variation in elevation look angles inherent in cross-track InSAR, *Prati and Rocca* [1993] developed a technique using multiple SAR surveys to improve the slant-range resolution and demonstrated an improvement of as much as 50% using SEASAT data. This technique has also shown improvement in the slant-range resolution using ERS-1 data [*Monti-Guarnieri et al.*, 1993(a); *Gatelli et al.*, 1994].

### **System Design / Implementation / Issues**

#### *Design Theory*

Design of an interferometric SAR, whether along-track or cross-track, must include an error budget (for examples see *Rodriguez and Martin* [1992], *Moccia and Vetrella*, 1992, *Zebker et al.* [1994(b)]). Issues to be considered include the decorrelation sources discussed earlier and uncertainties in the parameters directly affecting the measurement of the parameter of interest. As an example, consider the cross-track interferometric baseline. In reviewing (7), (8), and (9) it would seem that larger baselines would result in smaller height uncertainties. However this ignores both baseline decorrelation and phase aliasing that complicate the phase-unwrapping process [*Hagberg and Ulander*, 1993]. For cross-track InSAR, *Rodriguez and Martin* [1992] address the optimum baseline length and also define an optimum baseline-tilt angle, optimum bandwidth, and an optimum antenna length.

#### *Single-pass InSAR System Descriptions*

Several InSAR systems have been fielded since *Graham* [1974] first demonstrated the concept.

United Technologies Norden Systems has a Ku-band (16.2 GHz) two-dimensional InSAR flying on a Gulfstream II aircraft [*Held and O'Brien*, 1992; *Orwig and Held*, 1992; *O'Brien et al.*, 1994]. A single, large transmit antenna is located above a row of three along-track, receive-only antennas. The along-track receive antennas enable Displaced Phase Center Antenna (DCPA) techniques and along-track interferometry to be performed with radial velocity errors ranging from + 1 cm to +3 cm. Cross-track interferometry, accomplished by receiving through both the transmit antenna and the center receive-only antenna, provides pixel height estimates accurate to between 1.5 and 5 m. The system is VV polarized and has the capability to relocate moving targets (Doppler shifter) to their true position within a SAR image.

The Canadian Centre for Remote Sensing (CCRS) C- and X-band airborne SAR, which has been operated as a repeat-pass InSAR, has been modified such that the C-band (5.3 GHz) SAR can operate in single-pass, cross-track and along-track interferometric SAR modes [*Gray et al.*, 1992; *Gray and FarrisManning*, 1993; *Gray et al.*, 1994]. The system operates from a Convair CV-580 aircraft and the second receive antenna is H polarized. The vertical baseline is 2.807 m (with a baseline off-vertical angle of 40.61°), resulting in pixel-height errors ranging from 1.5 to 5 m. The horizontal baseline is 0.5 m,



resulting in a radial motion sensitivity of  $24^\circ$  per m/s and an unambiguous velocity range of  $\pm 7.5$  m/s.

The Naval Air Warfare Center (NAWC) / Environmental Research Institute of Michigan (ERIM) X-, C-, and L-band SAR has been modified such that both the X- and C-band systems have DPCA capability, enabling operation in the along-track InSAR mode [Schuchman et al., 1992]. The system, which operates on a P-3 aircraft, has a baseline of 0.7 m and an unambiguous velocity range of  $\pm 1.5$  m/s at C band.

The NASA JPL P-, L-, and C-band SAR (AIRSAR) was modified to perform C-band (5.6 cm) cross-track interferometry [Zebker et al., 1992(a)]. This system, known as TOPSAR, flies on the NASA DC-8 aircraft and is VV polarized. With a baseline of 2.58 m (and a baseline off-vertical angle of  $62.77^\circ$ ), systematic statistical pixel height errors in the 2- to 4-m range are possible, yet effects due to aircraft motion result in errors ranging from 3 m to 40 m, depending on the terrain.

Sandia National Laboratories has an airborne Ku-band (15 GHz) cross-track interferometric SAR (IFSAR) with a baseline of 0.2 m [Bicker and Hensley, 1994].

At least two spaceborne InSAR systems have been proposed as well. Moccia and Vetrella [1992] proposed a tethered InSAR system. To achieve pixel-height errors acceptable for 1:50000 scale topographic mapping, they propose using either an X-band system with a 100-m baseline or an L-band system with a 1000-m baseline.

A mission denoted as TOPSAT has been proposed to map the entire Earth in less than a year with an accuracy comparable to that of 1:50000 scale topographic maps [Zebker et al., 1994(b)]. The projected accuracy in elevation is 2 m and 30 m in both along-track and cross-track directions, with a swath width of 10.5 km. Radar frequencies in L band and Ku band are being considered, with the corresponding interferometric baseline lengths of about 1000 m and 15 m required to achieve the desired accuracy. Implementation at Ku band would require a single spacecraft, whereas L-band implementation would require dual spacecraft in parallel orbits.

#### Repeat-pass InSAR Demonstrations

Repeat-pass InSAR has been demonstrated using a variety of sensors, both airborne and spaceborne. These InSAR demonstrations are summarized below.

Gabriel and Goldstein [1988] produced an interferogram using data collected by the SIR-B SAR during selected portions of its crossed orbit geometry.

Several investigators [Goldstein, Zebker, and Werner, 1988; Li and Goldstein, 1990; Prati and Rocca, 1990; Prati, Giana, and Leuratti, 1990(a); Prati et al., 1990(b); Seymour and Scheuer, 1992; Zebker, Villasesnor, and Madsen, 1992(b); Zebker and Vollasesnor, 1992; Prati and Rocca, 1993] have used data collected from the SEASAT SAR to produce interferograms. For baselines ranging from 1000 m to 2000 m, statistical height accuracies ranging from 1.2 m to 1.6 m were obtained.

InSAR products have been produced using ERS-1 SAR images [Zebker Villasesnor, and Madsen, 1992(b); Askne and Hagberg, 1993; Goldstein et al., 1993; Massonnet et al., 1993; Monti-Guarnieri et al., 1993(a); Monti-Guarnieri, Prati, and Rocca, 1993(b); Kwok et al., 1994; Massonnet et al., 1994; Gatelli et al., 1994; Pasquali et al., 1994; Zebker et al., 1994(a)]. Others have simulated InSAR products using ERS-1 data [Hagberg and Ulander, 1993; Joughin and Winebrenner, 1994]. For baselines ranging from about 500 m to 1100 m, statistical height accuracies ranging from 1.5 m to 2.6 m were obtained.

Shinohara et al. [1992] simulated the performance of an InSAR using the JERS-1 SAR and found that for a baseline separation of 500 m, height errors ranging from 11 to 25 m could be expected.

Gray and Farris-Manning [1993] demonstrated repeat-pass interferometry at both C and X bands using the CCRS system that flies on a Convair 580. In a period of less than 2 hours SAR data were collected on multiple passes with equivalent horizontal baselines ranging from 2 m to 19 m. During the experiment, a radar reflector was moved between observations. Using interferometric techniques, reflector displacement was estimated and found to agree with actual displacements within 2 mm.

Finally, a repeat-pass interferogram has been proposed, using what would undoubtedly be the longest repeat-pass interval reported—more than 15 years. Using data collected from the spaceborne SEASAT SAR and airborne L-band SAR, Gatelli et al. [1994] have proposed to produce an interferogram of regions known for long-term stability, such as desert areas, to detect integrated tectonic motions.

## Applications

### Ocean Current Measurement

Goldstein and Zebker [1987] demonstrated the ability to measure ocean surface currents to a velocity resolution of 4 cm/s with the L-band InSAR on the NASA CV990 aircraft. Using the L-band NASA DC-8 InSAR, Goldstein, Barnett, and Zebker [1989] again measured ocean surface currents to a velocity resolution of 5 to 10 cm/s. Marom et al. [1990], Marom, Shemer, and Thronton [1991], Shemer, Marom, and Markman [1992], and Shemer and Marom [1993] showed that, using the L-band NASA DC-8 InSAR, the ocean surface current velocity and wavenumber spectra measurements can be obtained. Ocean surface wave velocities consistent with observed sea state were mapped by Schuchman et al. [1992], using the X-band NAWC/ERIM InSAR off the coast of Cape Hatteras.

Using interferometric techniques, Orwig and Held [1992], used the Norden Gulfstream II InSAR to show enhanced swells, wind waves, ship wakes and breaking surf along the coastline. They also used the moving target indicator (MTI) capability of the system to measure ship speed and position. Thompson and Jensen [1993] measured ship-generated internal wave velocities using the L-band NASA DC-8 InSAR. The



measured velocities were an order of magnitude larger than the in situ measured surface currents, however. This they attributed to different modulation strengths of surface Bragg waves advancing and receding from the radar.

Ocean-surface coherence-time measurement is possible using multiple-baseline along-track InSAR such that two independent measurements of the Interferometric velocity can be made and coherence times estimated. Using the three along-track receive-only antennas of the Ku-band Norden Systems InSAR, *Orwig and Held* [1992] estimated the ocean-surface coherence time to be approximately 5 ms at Ku band. *Carande* [1994] estimated ocean-surface coherence time at L band to be about 0.1 s, using the L-band NASA DC-8 InSAR. This was accomplished by operating the along-track InSAR in a dual-baseline mode; i.e., alternately using the forward and rear antennas as the transmit antenna and always using both on receive. In analyzing along-track InSAR system application for ocean current measurement, *Ouchi* [1994] indicates that, based on scene coherence time, an X-band system will be superior to an L-band one, as the former has a shorter integration time.

### **Topomapping**

An obvious application for cross-track interferometry is production of digital terrain models (DTM). Unlike stereo-pair radar techniques, where the observable terrain elevation is the order of the resolution cell size, the observable terrain elevation with InSAR is of the order of the radar wavelength [*Zebker et al., 1992*]. *Massonnet and Rabaute* [1993] examine the potential of using InSAR to produce industrial-quality terrain models and compare the DTM potential of various spaceborne SAR systems (including SEASAT, SIR-B, ALMAZ, ERS-1, and JERS-1). *Zebker et al.* [1994(a)] propose a spaceborne InSAR system capable of producing a topographic map of the entire Earth each year.

### **Earthquake-Displacement Monitoring**

Differential InSAR, capable of detecting elevation changes on the order of a radar wavelength, has been applied to earthquake-displacement mapping. First proposed by *Gabriel, Goldstein, and Zebker* [1989], this application has been demonstrated by *Massonnet et al.* [1993] and *Massonnet et al.* [1994] using ERS-1 SAR imagery collected prior to and following the 1992 earthquake in Landers, California. Through spatial averaging, a double-difference interferogram was produced with an elevation change precision of 34 mm on a grid spacing of 100 m that clearly showed the rupture zone.

### **Land Classification and Polar Monitoring**

*Askne and Hagberg* [1993] have explored the use of InSAR phase coherence as an element in classifying land surfaces, particularly open fields and forested areas. They have also explored the use of coherence as a change detection tool.

*Seymour and Scheuer* [1992] have demonstrated the possibility of applying repeat-pass InSAR in near-polar regions

despite numerous frozen and unfrozen waterbodies and varying weather conditions. *Goldstein et al.* [1993] have demonstrated the utility of InSAR in monitoring Antarctic ice-sheet-flow velocities using ERS-1 SAR data.

### **Conclusion**

By combining synthetic aperture radar and radar interferometry, many unique capabilities are presented through Interferometric SAR. When configured with the two receiving antennas vertically separated, high-quality terrain elevation mapping is possible. When these receiving antennas are separated horizontally, precise surface motions may be mapped. When an InSAR product, an interferogram, is produced from complex SAR images collected on separate passes, scene coherency can be measured. Applications of this technology include ocean surface monitoring (surface current velocity mapping, wave spectra, and ocean-surface coherence-time measurement), topographic mapping, terrain-surface-displacement mapping, land classification, and ice-sheet-flow monitoring. Both airborne and spaceborne demonstrations of this technology are reported.

### **References**

- Askne, J. and J. O. Hagberg, "Potential of Interferometric SAR for Classification of Land Surfaces," *Proc. of the 1993 Int. Geosci. and Remote Sens. Symp.*, Tokyo, Japan, 985-987, 1993.
- Bickel, D. L. and W. H. Hensley, "Interferometric SAR Phase Difference Calibration: Methods and Results," *Proc. of the 1994 Int. Geosci. and Remote Sens. Symp.*, Pasadena, CA, 2259-2262, 1994.
- Carande, R. E., "Estimating Ocean Coherence Time Using Dual-Baseline Interferometric Synthetic Aperture Radar," *IEEE Trans. on Geosci. and Remote Sens.*, 32(4), 846-854, 1994.
- Cattabeni, M., A. Monti-Guarnieri, and F. Rocca, "Estimation and Improvement of Coherence in SAR Interferograms," *Proc. of the 1994 Int. Geosci. and Remote Sens. Symp.*, Pasadena, CA, 720-722, 1994.
- Freeman, A., "SAR Calibration: An Overview," *IEEE Trans. on Geosci. and Remote Sens.*, 30(6), 1107- 1121, 1992.
- Gabriel, A. K. and R. M. Goldstein, "Crossed Orbit Interferometry: Theory and Experimental Results from SIR-B," *Int. J. of Remote Sens.*, 9(5), 857-872, 1988.
- Gabriel, A. K., R. M. Goldstein, and H. A. Zebker, "Mapping Small Elevation Changes Over Large Areas: Differential Radar Interferometry," *Journal of Geophysical Research*, 94(B7), 9183-9191, 1989.
- Gatelli, F., A. Monti-Guarnieri, F. Parizzi, P. Pasquali, C. Prati, and F. Rocca, "The Wavenumber Shift in SAR Interferometry," *IEEE Trans. on Geosci. and Remote Sens.*, 32(4), 855-865, 1994.
- Goldstein, R. M. and H. A. Zebker, "Interferometric Radar



- Measurements of Ocean Surface Currents," *Nature*, 328(20), 707-709, 1987.
- Goldstein, R. M., H. A. Zebker, and C. L. Werner, "Satellite Radar Interferometry: Two-Dimensional Phase Unwrapping," *Radio Science*, 23(4), 713-720, 1988.
- Goldstein, R. M., T. P. Barnett, and H. A. Zebker, "Remote Sens. of Ocean Currents," *Science*, 246, 1282-1285, 1989.
- Goldstein, R. M., H. Englehardt, B. Kamb, and R. M. Frolich, "Satellite Radar Interferometry for Monitoring Ice Sheet Motion: Application to an Antarctic Ice Stream," *Science*, 262(5139), 1525-1530, 1993.
- Graham, L. C., "Synthetic Interferometer Radar for Topographic Mapping," *Proc. of the IEEE*, 62(2), 763-768, 1974.
- Gray, A. L., K. E. Mattar, and P. J. Farris-Manning, "Airborne SAR Interferometry for Terrain Elevation," *Proc. of the 1992 Int. Geosci. and Remote Sens. Symp.*, Houston, TX, 1589-1591, 1992.
- Gray, A. L. and P. J. Farris-Manning, "Repeat-Pass Interferometry with Airborne Synthetic Aperture Radar," *IEEE Trans. on Geosci. and Remote Sens.*, 31(1), 180-191, Jan. 1993.
- Gray, A. L., M. W. A. van der Kooij, K. E. Mattar, and P. J. Farris-Manning, "Progress in the Development of the CCRS Along-Track Interferometer," *Proc. of the 1994 Int. Geosci. and Remote Sens. Symp.*, Pasadena, CA, 2285-2287, 1994.
- Guarino, C. R., "A Novel Method for Two-Dimensional Phase Estimation," *Proc. of the 1994 Int. Geosci. and Remote Sens. Symp.*, Pasadena, CA, 2279-2281, 1994.
- Hagberg, J. O. and L. M. H. Ulander, "On the Optimization of Interferometric SAR for Topographic Mapping," *IEEE Trans. on Geosci. and Remote Sens.*, 31(1), 303-306, 1993.
- Held, D. N. and J. D. O'Brien, "Norden Systems' 2-Dimensional Interferometric Synthetic Aperture Radar Flying Testbed," *Proc. of the 1992 Int. Geosci. and Remote Sens. Symp.*, Houston, TX, 646-648, 1992.
- Joughin, I. R. and D. P. Winebrenner, "Effective Number of Looks for a Multilook Interferometric Phase Distribution," *Proc. of the 1994 Int. Geosci. and Remote Sens. Symp.*, Pasadena, CA, 2276-2278, 1994.
- Just, D. and R. Balmer, "Phase Statistics of Interferograms with Applications to Synthetic Aperture Radar," *Appl. Optics*, 33(20), 4361-4368, 1994.
- Kwoh, L. K., E. C. Chang, W. C. A. Heng, and H. Lim, "DTM Generation from 35-Day Repeat Pass ERS-1 Interferometry," *Proc. of the 1994 Int. Geosci. and Remote Sens. Symp.*, Pasadena, CA, 2288-2290, 1994.
- Lee, J.-S. K. W. Hopple, S. A. Mango, and A. R. Miller, "Intensity and Phase Statistics of Multilook Polarimetric Interferometric SAR Imagery," *IEEE Trans. on Geosci. and Remote Sens.*, 32(5), 1017-1028, 1994.
- Li, F. K. and R. M. Goldstein, "Studies of Multibaseline Spaceborne Interferometric Synthetic Aperture Radars," *IEEE Trans. on Geosci. and Remote Sens.*, 28(1), 88-97, 1990.
- Lin, Q., J. F. Vesecky, and H. A. Zebker, "New Approaches in Interferometric SAR Data Processing," *IEEE Trans. on Geosci. and Remote Sens.*, 30(3), 560-567, 1992.
- Loffeld, O. and R. Kramer, "Phase Unwrapping for SAR Interferometry," *Proc. of the 1994 Int. Geosci. and Remote Sens. Symp.*, Pasadena, CA, 2282-2284, 1994.
- Madsen, S. N. and H. A. Zebker, "Automated Absolute Phase Retrieval in Cross-track Interferometry," *Proc. of the 1992 Int. Geosci. and Remote Sens. Symp.*, Houston, TX, 1582-1584, 1992.
- Madsen, S. N., H. A. Zebker, and J. Martin, "Topographic Mapping Using Radar Interferometry: Processing Techniques," *IEEE Trans. on Geosci. and Remote Sens.*, 31(1), 246-256, 1993.
- Marom, M., R. M. Goldstein, E. B. Thronton, and L. Shemer, "Remote Sensing of Ocean Wave Spectra by Interferometric Synthetic Aperture Radar," *Nature*, 345(6478), 793-795, 1990.
- Marom, M., L. Shemer, and E. B. Thronton, "Energy Density Directional Spectra of Nearshore Wave Field Measured by Interferometric Synthetic Aperture Radar," *J. of Geophys. Res.*, 96(C12), 22125-22134, 1991.
- Massonnet, D. and T. Rabaute, "Radar Interferometry: Limits and Potential," *IEEE Trans. on Geosci. and Remote Sens.*, 31(2), 455-464, 1993.
- Massonnet, D., M. Rossi, C. Carmona, F. Adragna, G. Peltzer, K. Feigl, and T. Rabaute, "The Displacement Field of the Landers Earthquake Mapped by Radar Interferometry," *Nature*, 364(6433), 138-142, 1993.
- Massonnet, D., K. Feigl, M. Rossi, and F. Adragna, "Radar Interferometric Mapping of Deformation in the Year After the Landers Earthquake," *Nature*, 369(6477), 227-230, 1994.
- Moccia, A. and S. Vetrilla, "A Tethered Interferometric Synthetic Aperture Radar (SAR) for a Topographic Mission," *IEEE Trans. on Geosci. and Remote Sens.*, 30(1), 103-109, 1992.
- Monti-Guarnieri, A., F. Parizzi, P. Pasquali, R. Prati, and F. Rocca, "SAR Interferometry Experiments with ERS-1," *Proc. of the 1993 Int. Geosci. and Remote Sens. Symp.*, Tokyo, Japan, 991-993, 1993(a).
- Monti-Guarnieri, A., R. Prati, and F. Rocca, "SAR Interferometric Quick-Look," *Proc. of the 1993 Int. Geosci. and Remote Sens. Symp.*, Tokyo, Japan, 988-990, 1993(b).
- O'Brien, J. D., H. Fullman, H. Holt, Jr., and L. Orwig, "Accuracy Validation of the IFSARE Radar System," *Proc. of the IEEE 1994 National Aerospace and Electronics Conference*, Dayton, OH, 234-238, 1994.
- Orwig, L. P. and D. N. Held, "Interferometric Ocean Surface Mapping and Moving Object Relocation with a Norden Systems Ku-Band SAR," *Proc. of the 1992 Int. Geosci. and Remote Sens. Symp.*, Houston, TX, 1598-1600, 1992.
- Ouchi, K. and D. A. Burrige, "Cross-Track and Proposed Multi-Frequency SAR Interferometry: Comparisons with Optical Holographic Interferometry," *Proc. of the 1994 Int.*



- Geosci. and Remote Sens. Symp.*, Pasadena, CA, 2263-2266, 1994
- Ouchi, K., "The Effect of SAR Bandwidth Ratio and Current Variation on Ocean Current Measurements by Along-Track SAR Interferometer," *Proc. of the 1994 Int. Geosci. and Remote Sens. Symp.*, Pasadena, CA, 723-725, 1994.
- Pasquali, P., R. Pellegrini, C. Prati, and F. Rocca, "Combination of Interferograms from Ascending and Descending Orbits," *Proc. of the 1994 Int. Geosci. and Remote Sens. Symp.*, Pasadena, CA, 733-735, 1994.
- Prati, C. and F. Rocca, "Limits to the Resolution of Elevation Maps from Stereo SAR Images," *Int. J. on Remote Sens.*, 11(12), 2215-2235, 1990.
- Prati, C., M. Giani, and N. Leuratti, "SAR Interferometry: A 2-D Phase Unwrapping Technique Based on Phase and Absolute Values Information," *Proc. of the 1990 Int. Geosci. and Remote Sens. Symp.*, Washington, D. C., 2043-2046, 1990(a).
- Prati, C., F. Rocca, A. Monti Guarnieri, and E. Damonti, "Seismic Migration for SAR Focusing: Interferometrical Applications," *IEEE Trans. on Geosci. and Remote Sens.*, 28(4), 627-640, 1990(b).
- Prati, C. and F. Rocca, "Improving Slant-Range Resolution With Multiple SAR Surveys," *IEEE Trans. on Aerospace and Electronic Systems*, 29(1), 135-144, 1993.
- Rodriguez, E. and J. Martin, "Theory and Design of Interferometric SARs," *Proc. of IKE*, 139(2), 147-159, 1992.
- Schuchman, R., A. Ochadlick, Cho, W. Dunlevy, J. Lyden, D. Lyzenga, and C. Wackerman, "Interferometric SAR Measurements Collected During the High Resolution Ocean Experiment," *Proc. of the 1992 Int. Geosci. and Remote Sens. Symp.*, Houston, TX, 458-461, 1992.
- Seymour, M. S. and T. E. Scheuer, "Aspects of Terrain Height Estimation using Interferometric SAR," *Proc. of the 1992 Int. Geosci. and Remote Sens. Symp.*, Houston, TX, 1573-1575, 1992.
- Seymour, M. S. and I. G. Cumming, "Maximum Likelihood Estimation for SAR Interferometry," *Proc. of the 1994 Int. Geosci. and Remote Sens. Symp.*, Pasadena, CA, 2272-2275, 1994.
- Shemer, L., M. Marom, and D. Markman, "Measurements of NearShore Ocean Currents Using Interferometric Synthetic Aperture Radar," *Proc. of the 1992 Int. Geosci. and Remote Sens. Symp.*, Houston, TX, 455-457, 1992.
- Shemer, L. and M. Marom, "Estimates of Ocean Coherence Time by Interferometric SAR," *Int. J. on Remote Sens.*, 14(16), 3021-3029, 1993.
- Shinohara, H., T. Homma, H. Nagata, H. Nohmi, H. Hirose, and S. Masuda, "Simulation of Interferometric Synthetic Aperture Radar Images," *Proc. of the 1992 Int. Geosci. and Remote Sens. Symp.*, Houston, TX, 1592-1594, 1992.
- Stevens, D. R., I. G. Cumming, M. R. Ito, and A. L. Gray, "Airborne Interferometric SAR: Terrain Induced Phase Errors," *Proc. of the 1993 Int. Geosci. and Remote Sens. Symp.*, Tokyo, Japan, 977-979, 1993.
- Stevens, D. R., I. G. Cumming, and A. L. Gray, "Motion Compensation for Airborne Interferometric SAR," *Proc. of the 1994 Int. Geosci. and Remote Sens. Symp.*, Pasadena, CA, 1967-1970, 1994.
- Tarayre, H. and D. Massonnet, "Effects of a Refractive Atmosphere on Interferometric Processing," *Proc. of the 1994 Int. Geosci. and Remote Sens. Symp.*, Pasadena, CA, 717-719, 1994.
- Thompson, D. R. and J. R. Jensen, "Synthetic Aperture Radar Interferometry Appl. to Ship-generated Internal Waves in the 1989 Loch Linnhe Experiment," *J. of Geophys. Res.*, 98(C6), 10259-10269, 1993.
- Ulaby, F. T., R. K. Moore, and A. K. Fung, *Microwave Remote Sensing Active and Passive*, Vol. 2, Reading, MA: Addison-Wesley, pp. 501-502, 620-621, 1982.
- Xu, W., E. C. Chang, L. K. Kwok, H. Lim, and W. C. A. Heng, "Phase Unwrapping of SAR Interferograms with Multifrequency or Multi-baseline," *Proc. of the 1994 Int. Geosci. and Remote Sens. Symp.*, Pasadena, CA, 730-732, 1994.
- Zebker, H. A. and R. M. Goldstein, "Topographic Mapping from Interferometric Synthetic Aperture Radar Observations," *J. of Geophys. Res.*, 91(B5), 4993-4999, April 1986.
- Zebker, H. A., S. N. Madsen, J. Martin, K. B. Wheeler, T. Miller, Y. Lou, G. Alberti, S. Vetrilla, and A. Cucci, "The TOPSAR Interferometric Radar Topographic Mapping Instrument," *IEEE Trans. on Geosci. and Remote Sens.*, 30(5), 9339-9340, 1992(a).
- Zebker, H. A., J. Villasenor, and S. N. Madsen, "Topographic Mapping from ERS-1 and SEASAT Radar Interferometry," *Proc. of the 1992 Int. Geosci. and Remote Sens. Symp.*, Houston, TX, 387-388, 1992(b).
- Zebker, H. A. and J. Villasenor, "Decorrelation in Interferometric Radar Echoes," *IEEE Trans. on Geosci. and Remote Sens.*, 30(5), 950-959, 1992.
- Zebker, H. A., C. L. Werner, P. A. Rosen, and S. Hensley, "Accuracy of Topographic Maps Derived from ERS-1 Interferometric Radar," *IEEE Trans. on Geosci. and Remote Sens.*, 32(4), 823-836, 1994(a).
- Zebker, H. A., T. G. Farr, R. P. Salazar, and T. H. Dixon, "Mapping the World's Topography Using Radar Interferometry: The TOPSAR Mission," *Proc. of the IEEE*, 82(12), 1774-1786, 1994(b).